Light transport through disordered layers of dense gallium arsenide submicron particles

T. van der Beek,[1,*] P. Barthelemy,[2] P. M. Johnson,[1] D. S. Wiersma,[3] and A. Lagendijk[1]

[1]*FOM-Institute for Atomic and Molecular Physics AMOLF, Science Park 104, 1098 XG Amste, The Netherlands*

[2]*Faculty of Applied Sciences, Delft University of Technology Lorentzweg 1, 2628 CJ Delft, The Netherlands*

[3]*European Laboratory for Non-Linear Spectroscopy (LENS) and CNR-INO, Sesto Fiorentino (Firenze), Italy*

(Received 20 December 2011; revised manuscript received 13 February 2012; published 1 March 2012)

We present a study of optical transport properties of powder layers with submicrometer, strongly scattering gallium arsenide (GaAs) particles. Uniform, thin samples with well controlled thicknesses were created through the use of varying grinding times, sedimentation fractionation, annealing, and a new sedimentation technique. These fabrication parameters were optimized to produce maximum scattering and minimum absorption. The physical properties were characterized using scanning electron microscopy (SEM) and x-ray diffraction. The optical transport mean-free path, absorption length, and the diffusion constant were determined for each sample using both continuous wave and time-resolved methods. The samples scatter strongly in the near infrared region. Total reflection and transmission measurements show that all of these samples have high absorption. X-ray diffraction results suggest that the source of this absorption is grinding induced strain and/or defects in the crystal structure. For all the different grinded GaAs powder samples that we investigated, the absorption length was less than ten micrometers.

DOI: 10.1103/PhysRevB.85.115401 PACS number(s): 42.25.Bs, 42.25.Dd, 42.25.Hz, 78.20.Ci

I. INTRODUCTION

Multiple scattering of light in turbid media is a subject of great interest in fundamental photonics research. Applications can be found in the coatings industry, biomedical imaging, remote sensing, and colloidal dynamics. Maximizing the opacity of layers while minimizing the thickness is an important aim for the paint and coatings industry as they try to minimize the use of often costly scattering materials.[1] Conversely, the solar cells industry uses light scattering and absorption in order to fabricate cells that efficiently trap light corresponding to the solar spectrum.[2] In biomedical imaging, layers of tissue blur transmission images because of scattering and absorption.[3] Understanding the trajectory of light inside turbid media reveals important information about the structure of the media as well as the nature of its interaction with light. In this study, we are particularly interested in extremely strong scattering, in the regime where the wavelength of the light is comparable to the transport mean free path and where the index of refraction contrast is maximal. In this strong scattering regime, there is the potential for interference to affect propagation, the extreme case being 3D strong localization of light or Anderson localization.[4–9]

In photonics research, there is an ongoing search for highly scattering materials in the optical regime.[10–12] The most strongly scattering low absorption materials at optical and near infrared wavelengths to date have been composed of high refractive index optically transparent materials with wavelength size microstructure, separated by a lower index medium. Examples are semiconductor materials with high refractive index contrasts and wide electronic band gaps such as TiO2, GaAs, GaP, Si, and Ge. These materials are either electrochemically etched or ground to a powder to enable multiple scattering. One advantage of powders is that the samples are optically isotropic. Another advantage is that they can be ground or fabricated to the desired size or infiltrated with a spacer. This makes it possible to tune the transport mean free path of a sample. Powders can also easily be combined and doped with dyes or other scatterers.

The preparation of homogeneous close packed powder slabs with low absorption is not trivial. Sedimentation followed by drying is a frequently used simple route to producing thin powder slabs. However, grains may aggregate during sedimentation, depending on their surface properties, which may reduce the homogeneity of the dried slab. Once dried, the powder slabs are fragile and may be easily displaced from the silica substrate. This property also makes characterization difficult. Light absorption can be introduced by the grinding process. It has been speculated that charged surface states can bind to for example CO_2, and defects or strain in the crystal can cause subband gap absorption.[13]

Rutile titanium dioxide (titania) powders have been used for numerous experiments requiring strong scattering and low absorption.[14,15] It is a semiconductor material with a refractive index of 2.7 and low absorption at optical frequencies. It is also easily obtained in wide variety of particle sizes and with different coatings because it is a common whitening agent for a number of industries, including coatings, cosmetics, and food products. A number of effects due to interference have been reported for titania powders including enhanced backscattering or weak localization,[16,17] long-range correlations,[18] and universal conductance fluctuations.[19] Anderson localization of light has also been reported for titania powders,[14,15] however, these claims were recently called into question by the same research group.[20] The observed time signatures may be experimental artifacts due to nonlinear responses from optical filters.

In the near infrared region, below the band-gap energy, gallium arsenide (GaAs) powder offers a higher index contrast than titania (3.6) and low (near) infrared absorption in bulk crystals. Indeed, Anderson localization has been reported for GaAs powders.[10] However, after the GaAs paper came out, there was a discussion about whether these phenomena were purely related to absorption in the sample.[11] The comments were countered in a reply[12] by pointing to inconsistencies in the arguments used by Scheffold *et al*. The issue of absorption versus localization in GaAs powders was nevertheless never fully resolved.

In this paper, results of a detailed study on the fabrication and the optical transport properties of ground gallium arsenide powder are presented. A new method to fabricate powder samples is presented, and a systematic way of characterization is developed. They were carefully characterized with SEM, profilometry, x-ray spectroscopy (EDS), and powder diffraction (XRD). In this way, the sample structure, uniformity, and thickness were characterized to remove ambiguity about the presence of voids, thickness variations, or particle aggregation effects.[21] A number of optical probes were used to distinguish dynamic and static properties, and to separate, for example, absorption from interference. The amount of subband gap light absorption and the mean-free path were determined by measuring the total transmission and total reflection simultaneously as a function of thickness. Position-dependent time-resolved transmission was used to probe for absorption and localization effects.[14,21–23]

The structure of this paper is as follows. First, the theory used to process the results is briefly presented followed by the methods and the section where the results are discussed. From these results, the mean-free path l, the absorption length L_a, and the diffusion constant D are determined and discussed in terms of optical optical absorption and Anderson localization.

II. THEORY

In this section, we quote the relevant light transport formulas with references to the theoretical and experimental foundations of each. All of the experiments involve coherent light impinging on one side of a slab of powder with diffuse light detected in transmission or reflection. The total diffuse transmission and reflection coefficients integrated over all angles are measured for the continuous-wave (cw) experiments. The slabs are approximated as semi-infinite since the thickness L of the samples under study is typically ~100 times less than the width.

In the limit of a large amount of scattering events far from sources and surfaces, the diffusion approximation sufficiently describes the transport of light intensity through a slab.[24] The diffusion model is an approximation of the radiative transfer equation, a transport model in which the phase of the wave is obviated. The two most relevant parameters from diffusion theory to this work are the absorption length L_a, describing the average depth penetrated before a photon gets absorbed, and the transport mean free path l, the average length before the propagation of the wave is randomized. We use the transport mean free path to approximate the penetration depth of the coherent beam.[21] The diffusion approximation is valid when $L \gg l$ and $L_a \gg l$. A third parameter, the extrapolation length z_e, is used to model the internal reflection of diffuse light at the sample-air interface. This parameter can be calculated using an approximation for the effective index of refraction n_{eff} of the sample.[25,26]

The total transmission, defined as the transmitted flux normalized by the incident flux, is given by[27]

$$T_d = \frac{1}{l}\int_0^L T_d(z_p)\exp\left(-\frac{z_p}{l}\right)dz_p, \tag{1}$$

where

$$T_d(z_p) = \frac{\frac{L_a}{l-L_a}\left[\exp\left(\frac{L}{L_a}-\frac{L}{z_p}\right)-1\right]\left[1+\frac{z_e}{L_a}\right]}{2\left(1+\frac{z_e^2}{L_a^2}\right)\sinh\left(\frac{L}{L_a}\right)+4\left(L_a^{-1}\right)z_e\cosh\left(\frac{L}{L_a}\right)} + \frac{\frac{L_a}{z_p+L_a}\left[\exp\left(-\frac{L}{L_a}-\frac{L}{z_p}\right)-1\right]\left[1-\frac{z_e}{L_a}\right]}{2\left(1+\frac{z_e^2}{L_a^2}\right)\sinh\left(\frac{L}{L_a}\right)+4\left(L_a^{-1}\right)z_e\cosh\left(\frac{L}{L_a}\right)}. \tag{2}$$

Here, $T(z_p)$ is the diffuse transmission from a delta function source at depth z_p. It is assumed that the direction of the wave is randomized after an average distance l, and that the scatterers can be approximated as isotropic scatterers. In the limit of thick, absorbing samples ($L \gg L_a$), Eq. (1) reduces to a simple exponential decay:

$$T_d = \frac{2L_a(l+z_e)}{L_a^2+2z_eL_a+z_e^2}\exp(-L/L_a). \tag{3}$$

The total reflection gives

$$R_d = \frac{1}{l}\int_0^L R_d(z_p)\exp\left(-\frac{z_p}{l}\right)dz_p, \tag{4}$$

where

$$R_d(z_p) = \frac{-\frac{L_a\exp(-\frac{L}{L_a})}{l+L_a}\left[\exp\left(-\frac{L}{L_a}-\frac{L}{z_p}\right)-1\right]\left[1+\frac{z_e}{L_a}\right]}{2\left(1+\frac{z_e^2}{L_a^2}\right)\sinh\left(\frac{L}{L_a}\right)+4\left(L_a^{-1}\right)z_e\cosh\left(\frac{L}{L_a}\right)} - \frac{\frac{L_a\exp(-\frac{L}{L_a})}{z_p-L_a}\left[\exp\left(\frac{L}{L_a}-\frac{L}{z_p}\right)-1\right]\left[1-\frac{z_e}{L_a}\right]}{2\left(1+\frac{z_e^2}{L_a^2}\right)\sinh\left(\frac{L}{L_a}\right)+4\left(L_a^{-1}\right)z_e\cosh\left(\frac{L}{L_a}\right)}. \tag{5}$$

In the limit of thick, absorbing samples ($L \gg L_a$), Eq. (4) reduces to a simple exponential decay:

$$R_d = \frac{L_a(L_a+z_e)}{L_a^2+2z_eL_a+z_e^2}\exp(-z_p/L_a). \tag{6}$$

Energy conservation requires that

$$A = 1-(T_d+R_d+T_{\text{bal}}), \tag{7}$$

where A is the absorptance, or the fraction of light absorbed in the sample, and T_{bal} is the ballistic transmission. The ballistic transmission is described by an exponential decay with the optical thickness:

$$T_{\text{bal}} = \exp(-L/l). \tag{8}$$

The extrapolation length at the slab interface z_e depends on the internal reflectivity of the sample interface and is described by[26]

$$z_e = \frac{2}{3}l\frac{1+\overline{R}}{1-\overline{R}}, \tag{9}$$

where $\overline{R}$ is the average reflectivity of the sample interfaces. The extrapolation length becomes an increasingly influential parameter on the transmission coefficient as the effective refractive index n_{eff} of a material becomes higher. The effective reflective indices were estimated with the Bruggeman effective medium theory.[28]

In the regime of strong localization, the diffusion of light comes to a halt, due to strong interference of the electromagnetic waves that undergo multiple scattering inside

the sample. It has been suggested theoretically[22] and demonstrated experimentally[22,23] that the slowdown of diffusion can be modeled with a time-dependent diffusion constant. This behavior can be observed experimentally with a time-resolved transmission measurement. In the absence of localization, the time-resolved transmission will decay exponentially due to both scattering and absorption. Deviations from this single exponential behavior points to Anderson localization.

The diffuse intensity decays exponentially with a time constant τ that depends on the diffusion constant and the absorption length and the effective sample thickness $(L + 2z_e)$:[29]

$$\frac{1}{\tau} = D\left[\left(\frac{\pi}{L+2z_e}\right)^2 + \left(\frac{1}{L_a}\right)^2\right]. \tag{10}$$

In addition to the expressions for modeling the optical data, we also present here one expression for modeling the sample characterization using x rays. In x-ray diffraction crystallography measurements, instrumental factors, the size dislocations and strain differences influence the line width. The following formula, known as the Scherrer formula,[30] relates the linear dimension of the particle d to the line broadening β at the FWHM:

$$d = \frac{K\lambda}{\beta\cos(\theta)}, \tag{11}$$

where θ is the incident angle, K the shape factor, and λ is the wavelength of the incident x rays. This formula will be used to estimate domain sizes in the ground samples, thereby giving information about the presence of grinding-induced structural changes inside the GaAs powders.

III. METHODS

A. Sample fabrication

We present here detailed descriptions of the fabrication of semiconductor powder slabs for optical experiments. The fabrication goal was to make smooth samples of different layer thickness with homogeneous particle distribution with submicrometer size. A secondary goal was to reduce the amount of light absorption by conserving or recovering the crystallinity of the particles. The sample fabrication starts with the grinding of GaAs single-crystal (100) wafers. The resulting powder was divided into fractions of different particle sizes. Some of these batches were annealed to reduce the defects introduced during the fabrication process. One particle size range was selected, to sediment layers with onto a glass substrate. A novel sedimentation method, described below, was developed and used to produce homogeneous slabs.

Undoped 51 × 0.5 (diameter × thickness) mm GaAs (100) wafers were purchased from MTI Corporation. A ball mill (Pulverisette 7) was used to grind the wafer into powder in an ethanol suspension at 1000 rpm. To be able to grind hard and brittle solids such as GaAs, a hard mill beaker was selected. Grinding in steel beakers and marbles were compared to a zirconium oxide beakers and marbles. Since both types of beakers produced submicrometer powders within 5 minutes of grinding time, steel beakers were used for the remainder of the experiments. 30 ml of an organic solvent, typically ethanol, was added to the GaAs to ensure an even distribution of the particles during grinding.

The stress in the crystal structure of the GaAs was intentionally held to a minimum by using short grinding times. Typically, the GaAs is ground during five minutes. The size distribution was narrowed using repeated gravity sedimentation in ethanol. Typically, 5.7 g of GaAs powder were dispersed in 10 ml ethanol, stirred, and then left to sediment for one minute. The top 20% layer was pipetted off and redispersed in another 10 ml of ethanol. This method was repeated until the desired particle size distribution was extracted.

Some of the ground and selected powders underwent an additional annealing step in an effort to reduce the strain in the crystal and to remove adsorbed molecules. These samples were heated to 700 °C and at 900 °C in a vacuum oven for four hours in a ceramic holder. The temperature was probed at the site of the powder. The results for these samples are presented in the Appendix B.

The GaAs particles were then deposited onto a glass substrate. 150 μm thick, 1 cm diameter round hydrophilic microscope slides were used as substrate. For some of the substrates, a 500 μm wide, 20 nm thick ring of gold was sputtered onto the edge of the microscope slide. This gold ring provided the conductive contact between the powder and the SEM sample holder to drain the excess electrons causing area charging. This ring was only deposited at the edge of the substrate, so it did not interfere with the optical measurements.

In order to produce uniform layers of dry powder of various thickness, a total of four deposition techniques were investigated. Three of these techniques are common laboratory practice. The fourth was developed by us as a means of improving on these previous techniques. The first technique investigated was the so-called drop drying deposition technique, used previously on GaAs powders[10,13] to make optically thin layers. Typically, 1 mg of ground GaAs powder was suspended in 1 ml ethanol. A pipette sucks up the slurry, and deposits one or more drops unto the substrate before leaving it to dry. The second technique investigated was the blade edge spreading method.[31] The GaAs slurry was distributed evenly on the edge of a conventional razor blade. With an angle of 30°, and the slurry side down, the blade was used to spread the powder evenly onto the glass surface. The thickness could be varied by varying the distance between the blade and the surface of the substrate or by changing the concentration of the slurry. The third technique investigated was airbrush spraying, as is used to make homogeneous coating surfaces. A 0.3 g/l GaAs ethanol slurry was treated with ultrasound in an ultrasonic bath for 30 minutes to break up aggregates and ensure dispersion of the powder in the solvent. A needle airbrush was filled with the mixture, and sprayed onto the vertically attached substrate using a 3 bar nitrogen feed. This was done in a dispensable glove box compartment for safety considerations. The sprayed substrate was left drying horizontally to prevent dripping. These three techniques did not produce samples of necessary uniformity at all required thicknesses. These issues are discussed in the results section.

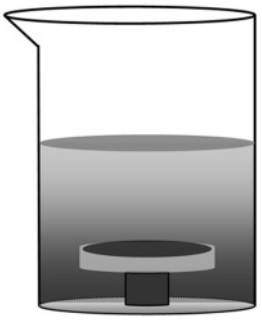

FIG. 1. Sketch of the slow sedimentation method. The GaAs powder/ethanol slurry is depicted by the gray turbid area. The round shaped glass substrate (150 μm thickness, 1 cm diameter) is elevated from the bottom of the beaker by placing it on a smaller cylinder. After sedimentation, the rest of the ethanol was allowed to dry while the sample remains horizontal.

We ultimately developed a different method to improve the sample quality. The technique is illustrated in Fig. 1. The circular glass substrate is supported by a cylinder. The cylinder has a smaller diameter than the glass substrate. The edges of the substrate are freely suspended in the dispersion. A 0.05 g/l GaAs ethanol slurry was poured into a beaker with the glass substrate. The distance between the substrate surface and the suspension surface was typically in the order of 7 cm. The monodisperse powder was left to sediment down unto the substrate. The ethanol was left to evaporate in air at room temperature over a period of roughly 10 h. The thickness of the powder layer could be controlled by changing the concentration of the suspension and by varying the distance between the glass substrate and the bottom of the flask.

In addition to the GaAs samples, a series of nonabsorbing reference titania samples of different thickness were also fabricated. A commercially available powder was used (Dupont Ti-Pure 902+). These titania powder particles have a mean size of 0.4 μm and are coated with alumina and silica to stabilize them in dispersions. This particle size compares to the smallest GaAs powder particles used in this study. The slabs of titania were prepared in the same fashion as the GaAs powder samples for optimal comparison.

B. Sample characterization

Scanning electron microscopy (SEM), profilometry, x-ray diffraction crystallography, and energy dispersive x-ray spectroscopy were used to characterize the thickness, particle shape, particle size, purity, and polydispersity of GaAs powder samples.

Scanning electron microscopy (SEM) was used to image nondestructively the semiconducting samples with sub micrometer resolution. The SEM micrographs (FEI XL30 microscope) were used to characterize the particle size distribution and the particle shapes. The micrographs also provided characterization of thickness deviations, pits, or holes. The particle sizes were estimated by matching a circle of approximately the area of the particle on the micrograph by eye. The resulting diameter was used as a measure for the 3D particle size. For each micrograph, all particles within an area of approximately 400 μm^2 were analyzed. For particle diameters smaller than 100 nm diameter, a separate high-resolution SEM photo was used, and a smaller area analyzed. This analysis provided sizes for roughly 700 to 1000 particles per micrograph from which a histogram could be composed. Two histograms were computed for each SEM. The occurrence histogram gives the number of particles found within each diameter bin normalized by the total number of particles counted. The volume fraction histograms give the total volume of particles within diameter bin normalized by the total volume of particles calculated. These histograms are presented in the results section. Macroscopic features could be observed by tilting the sample inside the SEM. Some slabs have regions with inhomogeneities alternated with smooth regions. For this reason, all the samples used for the optical experiments were fully characterized over the entire area of the samples. If there were inhomogeneities on the sample surface, these were avoided by appropriately aligning the optical measurement.

The thickness of the layer was determined using a profilometer. First, an approximately 150-μm wide scratch was made with a scalpel in the powder layer to expose the glass substrate underneath. Thickness profiles were measured using a profilometer KLA Tencor Alpha Step 500 by running the needle perpendicular to the scratch. The stylus was run across the scratch at 10 μm/s and a low stylus force of 13.1 mg was used so as not to displace the powder layer. The resulting U-shaped profile provided nanometer resolution thickness measurement in a scanned area of approximately 400 μm. It gives a quantitative indication of the surface smoothness around the scratch. The thickness was checked for consistency with an optical microscope by focusing and defocusing a microscope objective across the scratch. The two methods gave consistent results.

Two x-ray based methods were used to detect chemical impurities and crystallinity of the powders. X-ray diffraction spectra were made of the GaAs powder samples to evaluate the crystallinity, and the presence of strain or defects introduced during the grinding process. The GaAs monocrystalline wafer was used as a reference for the latter measurement. Contamination of the samples was examined in the SEM with energy dispersive spectroscopy (EDS). The average detection limit for impurities relative the quantities of gallium and arsenide is $\approx$0.1%.

C. Optical measurements

The total transmission and total reflection measurements provided a reliable means of determining the light absorption and diffusion in a slab. The transport mean free path and the absorption length could be determined by varying the thickness of the samples.

The total transmission and reflection setup is illustrated in Fig. 2. The setup allows for both transmission and reflection to be measured without moving the detector or sample position, thus minimizing measurement artifacts. It consists of a gold coated integrating sphere, a broadband source (Fianium SC-450-2) and a vis-NIR spectrometer (Ocean Optics, 0.95–1.7 μm). The sample is positioned in front of the integrating sphere. The visible wavelengths absorbed by GaAs are blocked

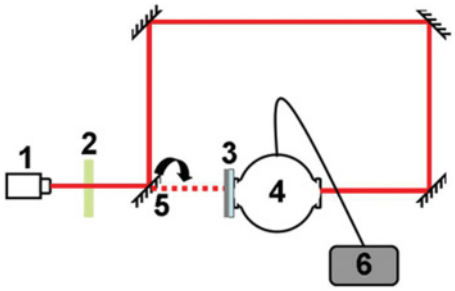

FIG. 2. (Color online) Schematic description of the setup used to measure the total transmission and the total reflection. (1) is the white light super continuum laser, (2) is the 1000-nm low-pass filter. The sample (3) is attached to the front side of the integrating sphere (4). A flipping mirror (5) is used to switch between the total transmission and total reflection measurement. For the total reflection measurement, the laser light is diverted with four mirrors to the backside of the integrating sphere. The light is collected at the top of the sphere with a fiber and processed by a fiber spectrometer (6).

using a low-pass filter. The geometry of the setup is such that the transmission measurement is a measure of both the diffuse and the ballistic transmission ($T + T_{\mathrm{bal}}$). The sum of the normalized transmission and reflection determines the total absorptance [see Eq. (7)].

D. Time-resolved transmission and reflection

To measure the time-dependent behavior of the GaAs powder samples, a sum-frequency cross correlation method was used. The setup is based on the optical gating technique described in Ref. 32 and is diagramed in Fig. 3.

A Tsunami 810-nm, 150-fs Ti-Sapph pulsed laser is split into a sample beam (lower beam path in the diagram) and a reference beam (upper path in the diagram). The sample beam pumps an optical parametric oscillator to produce 1.5-μm near-infrared pulses. A 25-mm focal lens collects the transmission, which is superimposed with the pump beam. A BBO nonlinear crystal combines the two beams for sum-frequency generation. The intensity of the sum-frequency is measured in a photomultiplier tube.

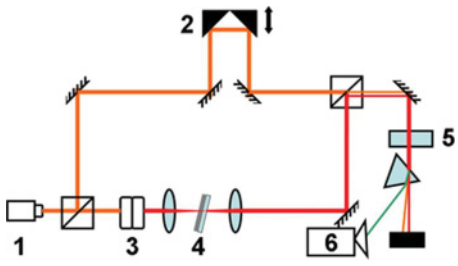

FIG. 3. (Color online) Schematic description of the optical gating technique. A Ti-Sapph laser beam (1) is split into a sample beam (below) and a reference beam (above). The reference beam passes through an automated delay line (2). The sample beam pumps an OPO (3) before hitting the sample (4). The lenses surrounding the sample are used to change the focus on the sample and coming out of the sample. The two beams meet in a BBO Crystal (5). The sum-frequency signal is filtered with a prism and collected in a PMT (6). A chopper and a lock-in amplifier were used to reduce the noise; they were omitted in the schematic drawing for clarity.

To avoid heating up an absorbing sample with the impinging beam, we placed the sample before the focus. The beam spot diameter is approximately 50 μm. As a consequence, the transmission results represents an average of the photons traveling through pores and diffusing through the surrounding dense powder assembly.

IV. RESULTS

A. Nonoptical sample characteristics

We show in Fig. 4 that we were able to accurately determine the particle size distribution of the sample with the SEM images. Figure 4(a) is a micrograph of the nonfractionated powder, Fig. 4(b) of the smallest particles removed after one fractionation step, and Fig. 4(c) is the largest particles

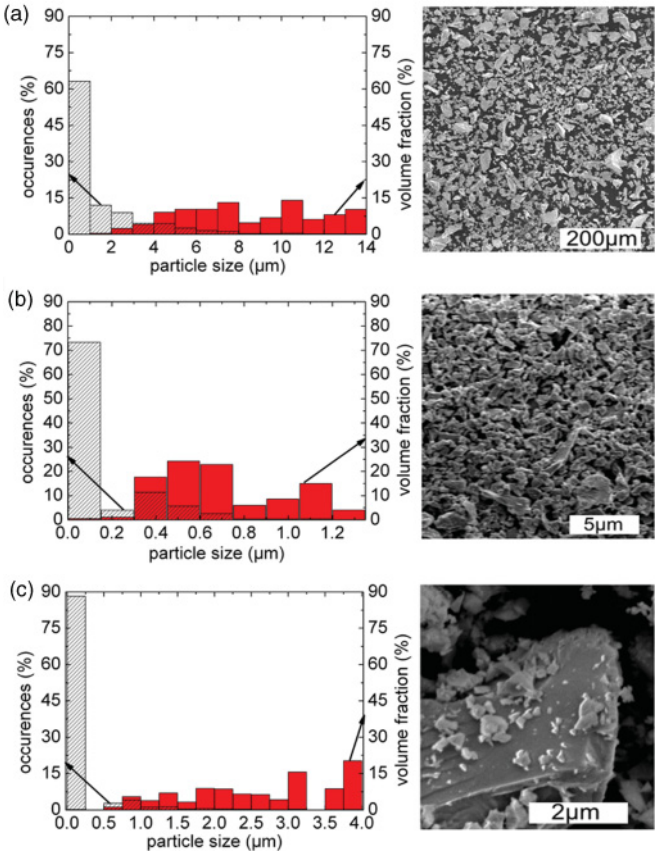

FIG. 4. (Color online) Histograms and corresponding SEM images for different steps in the fractionation process. The occurrence histogram (patterned columns) depicts the amount of particles of a certain size or counts, and the volume fraction histogram (solid red columns) is the volume fraction per particle size. The white rectangles in the SEM images are the scale bars with length in micrometers. (a) The ground powder before sedimentation fractionation. (b) The powder after fractionation for optimally small particles sizes. This sample was used for the optical experiments described in this article. (c) The remaining sediment after producing sample b, with an additional step of removing the largest particles. The SEM image in (c) is a higher resolution scan allowing smaller particles to be counted.

twice fractionated to remove small particles. The shape of the particles can be described as multifaceted random structures with sharp edges. Both the occurrence (patterned columns) and volume fraction (solid red column) histograms are shown in each figure. From the occurrence histogram, it becomes clear that small particles of sizes between 100 and 500 nm were still present in all analyzed samples. This is also illustrated in the SEM image in Fig. 4(c). However, these particles represent a negligible volume fraction of the particles, as seen in the volume fraction histograms. It is possible that these particles are only present on the surface of the sample as they sediment orders of magnitude more slowly than the other particles for all samples, or that they have aggregated irreversibly to the larger particles. The particle sizes in the original dispersion [see Fig. 4(a)] vary between 0.1 and 14 μm. The volume fraction was evenly distributed in this range. As seen in Figs. 4(b) and 6, the particle size fractionation method worked effectively to isolate small sized ($<$1.3 μm) ground GaAs particles [see Fig. 4(b)], and to isolate larger particles [see Fig. 4(c)]. The powder depicted in Fig. 4(b) is the ground GaAs powder batch that is used for all the experiments described in this paper. The mean particle size in all samples can thus be deduced from the volume fraction histogram: 0.7 ± 0.5 μm where the last number is the standard deviation.

We compared airbrush spraying, drop deposition, and the slow drying technique for deposition of the powder onto the glass substrate. For thin layers ($\leqslant$5 μm), the airbrush spraying technique provided well dispersed samples. Thicker layers of powder could not be made because the force of the spray displaced the particles that were already deposited on the substrate. The samples made with the drop deposition technique showed inhomogeneous thickness distributions on surfaces in the SEM. Reducing the volume fraction of particles did not improve the sample quality. It appears that the dynamics of the droplet drying process deposits the smallest particles near the edges of the sample, inhomogeneously distributing the different sample sizes over the surface of the substrate. The slow drying technique successfully solved this problem, creating homogeneous, uniform samples. We attribute this improvement to the change in the geometry of the drying front at the glass substrate and the low concentration of the suspension.

The filling fraction could not acurately be determined directly from the SEM images or particle size distributions. The SEM images show no evidence of unusual packing of the particles. We took a rough estimate for the total GaAs volume fraction of $f = 0.5$ to calculate the mean effective refractive index $n_{\text{eff}} = 2.2$ at 1.5 μm.

The GaAs powder raw EDS spectrum is shown in Fig. 5. The peaks can be assigned to all the expected chemical elements: gallium, arsenic, and oxygen adsorbed onto the powder. The carbon (C) peak in the EDS measurement comes from the adhesive layer used to attach the powder to the sample holder. We have marked the location in the spectrum of iron peaks to confirm the absence of possible impurities originating from the grinding process. The grinding and further processing of the GaAs powder did not add any impurity that could be detected by EDS.

The XRD spectrum of the ground GaAs powder showed diffraction peaks that can be attributed to the crystalline planes

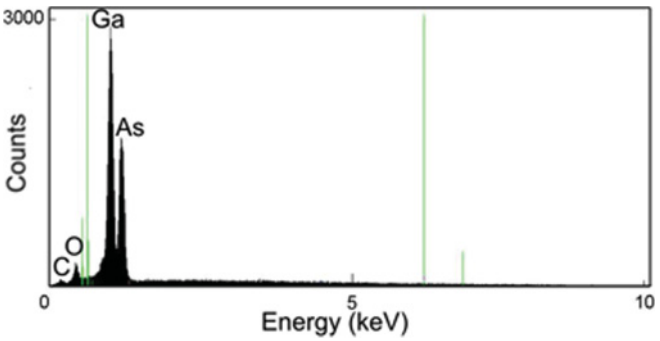

FIG. 5. (Color online) Energy dispersive spectroscopy (EDS) measurements of the purity of the GaAs powder. The C peak is originated from the sample holder. The green lines show the positions of absent iron peaks, expected to appear after grinding in steel recipients.

of GaAs: $2\theta = 27.5^\circ$ [GaAs (111), 45.0° (GaAs (220)], 54.0° [GaAs (311)]. Figure 6 gives x-ray scattering data from a single-crystal GaAs wafer (narrow peaks) and of a GaAs powder sample [broad peaks of the GaAs (004)] between $2\theta = 65.5^\circ$ and 67.5°. The double peaks for each sample originate from the copper K-α emission lines. The peaks for both the crystal and the powder have measurable widths, with the width of the powder scan being noticeably wider than that of the single crystal. The theoretical width of a large (mm scale) single crystal of GaAs is much narrower than either of the peaks shown. Therefore we can attribute the width of the single crystal data to instrumental resolution (triangular data points in Fig. 6). The powder sample therefore shows a

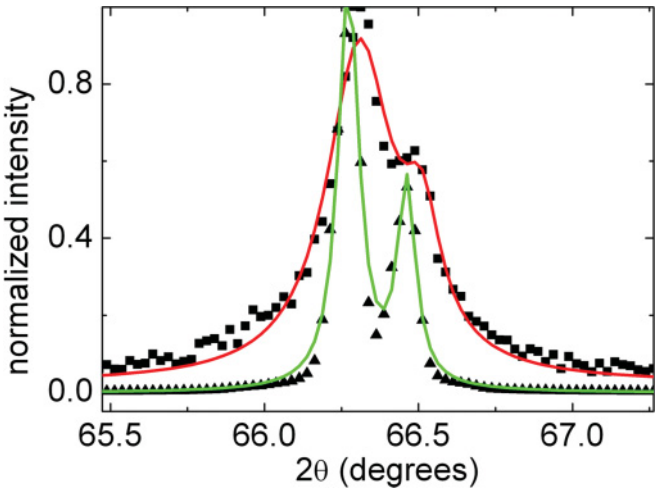

FIG. 6. (Color online) X-ray crystallography (004) GaAs plane peaks for a ground GaAs powder sample (solid squares) and a GaAs single-crystal slab (solid triangles) showing broadening due to grinding. The peaks are normalized to the largest (Cu K-α1) peak centered at $2\theta = 66.2$ degrees. The origin of the other half of the doublet at $2\theta = 66.5$ degrees is the copper K-α2 emission line from the x-ray source. The powder peak maximum is approximately one-third smaller than the maximum in the GaAs. The red and green solid lines are Lorentzian fits of the two peaks for the powder and the GaAs wafer, respectively. The width of the peak is an indication for instrumental resolution and/or the mean domain size in the crystallites.

broadening beyond the instrumental resolution. We attribute the increase of the peak widths to strain and/or defects in the crystal. The solid lines through the data in Fig. 6 are Lorentzian fits through both data sets, each fit consisting of a sum of two Lorentzians to account for the Cu source K-α splitting. The GaAs powder peak is approximately 1.4 times broader than the wafer peak. The broadness extracted from the fitted peaks are used in the Scherrer formula Eq. (11) with the estimated shape factor of 0.9 and the x-ray wavelength 1.54 Å to obtained mean domain size τ of 38 nm. This domain size is a factor 18 smaller than the mean particle size determined from SEM images. We can conclude that grinding has introduced domains and/or strain in the grains of powder that result in a broadening of the x-ray peaks. These domains may also be responsible for some of the optical properties that we will describe below.

B. Optical measurements

Eight well characterized GaAs ground powder samples in a range of thicknesses between 7 and 35 μm were used for the optical measurements. The raw data of the optical total transmission and total reflection spectra of one GaAs powder sample of 13-μm thickness is plotted in Fig. 7. The inset shows the reference measurement of a rutile titania sample of 80 μm thickness to which the GaAs measurements was normalized. Rutile titania is considered to be nonabsorbing in the wavelength range of interest: 900 nm $< \lambda <$ 1700 nm. The bottom lines (red solid) are the total transmission spectra, the middle lines (blue dashed) are the total reflection spectra and the top lines (black solid) are the sums of the two. The small contribution of the ballistic transmission [see Eq. (8)] is included in the solid transmission line. The total transmission, reflection, and the sum of GaAs powder are roughly constant above $\lambda = 1200$ nm and then begin to decrease as they approach the intrinsic electronic band-gap wavelength of GaAs ($\lambda = 870$ nm).

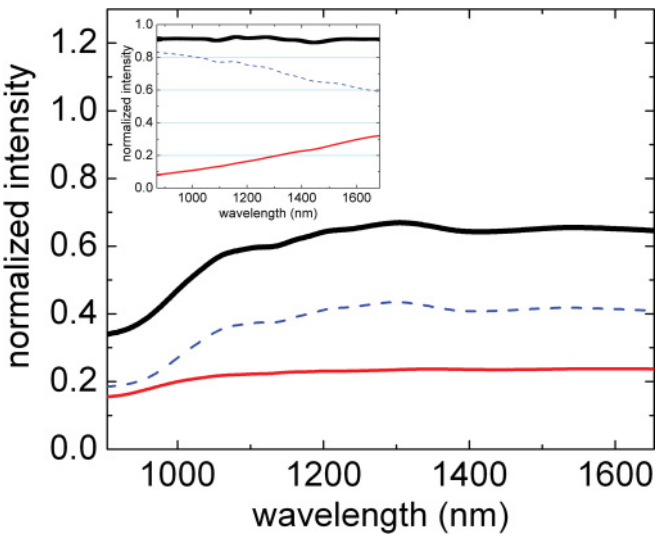

FIG. 7. (Color online) Total transmission (red solid line) and total reflection (blue dashed line) spectra of a 13-μm ground GaAs powder and of a reference titania sample (inset). The top black solid lines are the sum of the wavelength-dependent total transmission and total reflection data of a GaAs powder sample and the reference titania sample.

The reflection and transmission of the titania sample depend strongly on wavelength. This is due to the small size of the particles and to the strong dependence of the scattering cross section on wavelength. The calculated titania transmission and reflection sum of 0.91 (the thick black line) is constant throughout the studied wavelength region. It is known that titania absorbs very little at these wavelengths. Therefore, the actual value for the sum in titania should be closer to 1.0. The unaccounted for light has likely been lost to the sample holder, which does not make a completely flush fit to the integrating sphere. It should be noted that the titania sample is a factor 8 thicker than the GaAs powder sample (80 μm compared to 13 μm), again indicating absorption in GaAs compared to titania. When normalized to the titania measurement, the GaAs powder absorptance at $\lambda = 1.5$ μm, is 0.44, or 44% of the light at that wavelength is absorbed by a 13-μm ground GaAs powder sample.

We compare the absorptance of different ground GaAs powder samples at $\lambda = 1500$ nm in Fig. 8. The absorptance increases as the thickness of the sample increases to a constant value for thicknesses greater than 20 μm. This can be understood as an exponential drop in the total transmission over a length scale on the order of the absorption length. For thick enough samples, the reflection contribution dominates the transmission, therefore the absorptance becomes independent of thickness and plateaus at $A = 0.47 \pm 0.05$. This plateau is given by the dashed line in the plot. The error bars are obtained by repeating the measurement on different positions of the sample. The error bars become larger for thinner samples because these are more sensitive to inhomogeneities. The solid

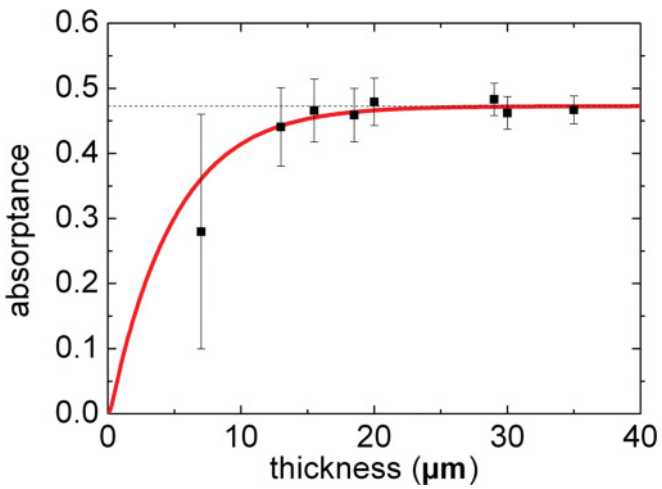

FIG. 8. (Color online) The absorptance at wavelength 1500 nm of GaAs powder samples of different thicknesses is plotted. The squared points are the absorptance measurements [see Eq. (7)] for samples of different thicknesses. The intercept with dashed horizontal line represents the region where the GaAs samples are so thick that transmission is nearly reduced to zero. The fit to the sum of Eqs. (2), (5), and (8) yields an absorption length of 6.1 ± 1.9 μm and a transport mean free path of 0.6 ± 0.2 μm. From the horizontal dashed line, the limit of the absorptance at large sample thickness, the mean total reflection from a thick GaAs powder slab can be read 0.53 ± 0.10.

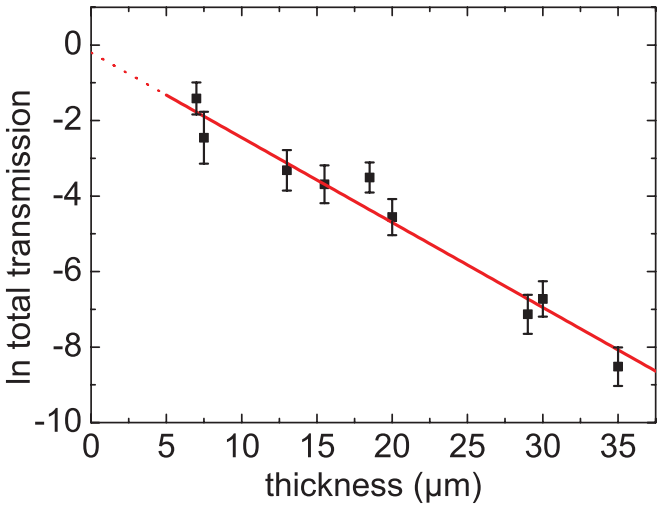

FIG. 9. (Color online) Total transmission through GaAs powder samples of different thicknesses at light source wavelength 1500 nm. The red line is a fit through the data points to Eq. (3). From the slope we obtained the absorption length, $L_a = 4.4 \pm 0.3$ μm.

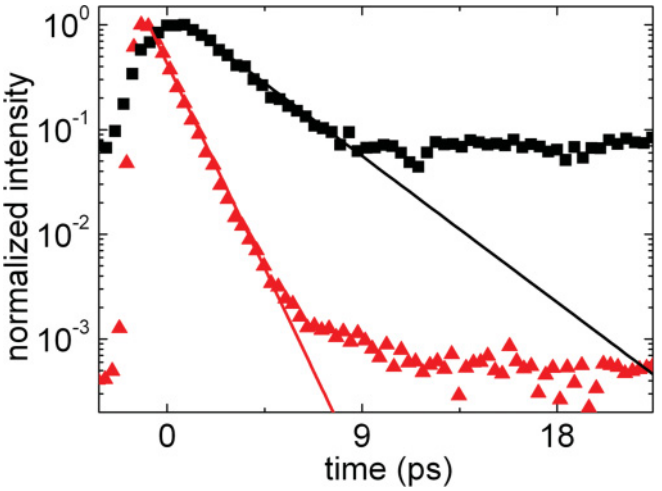

FIG. 10. (Color online) Time-resolved transmission measurement of GaAs powder samples of different thicknesses. The black squares with the red exponential fit line represent the 14-μm sample and the red triangles with the black fit the 7-μm sample. The peak maxima are normalized to make a visual comparison of the decay slopes easier. The single exponential fits of the slopes (lines in the graph) are expressed as the decay time τ, inversely proportional to the diffusion constant. The decay times are $\tau = 2.8 \pm 1.0$ ps for the 14 μm sample, and $\tau = 1.0 \pm 0.4$ ps for the 7 μm sample.

red line in the figure is the best fit of the theoretical value of A given by combining Eqs. (2), (5), and (8) with Eq. (7). The absorption length L_a and the transport mean free path l are the free parameters. We calculated the extrapolation length relative to the mean free path using Eq. (9) to obtain $z_e = 7l$. Changing the filling fraction to 30% in this calculation did not change the resulting absorption length or the transport mean free path beyond the error bars. The fitted curve is horizontal when the sample is thicker than 24 μm. From the fit, we obtained the absorption length of 6.1 ± 1.9 μm and the transport mean free path is 0.6 ± 0.2 μm.

The thickness dependence of the total transmission at $\lambda = 1500$ nm in the GaAs powder slabs is plotted separately in Fig. 9. We used a natural logarithmic scale for the total transmission to highlight the exponential behavior of the light transport through the slab, and to draw the attention to the intercept with the vertical axis. The error bars are a measure for the reproducibility from one region to another in the sample. The solid line is Eq. (3) fitted through the data points. The slope gives the inverse of the absorption length, and the intercept with the vertical axis is an indication for the transport mean free path. We find $L_a = 4.4 \pm 0.3$ μm and $l = 0.7 \pm 0.1$ μm, consistent with the fitted values with error bars in Fig. 8. The extrapolation length z_e is assumed seven times the transport mean free path. The diffusion equation in the limit where $L_a \ll L$ [see Eq. (2)] describes the total transmission in ground GaAs powder well. We conclude that the continuous-wave transport of light at $\lambda = 1500$ nm is well described by the diffusion approximation with strong absorption. Interference effects can be neglected.

Two time-resolved transmission curves of ground GaAs powder samples of different thicknesses are plotted in Fig. 10. The maxima of the peaks are normalized to one to make the comparison of the two curves easier. The intensity (y axis) is scaled logarithmically. The horizontal axis is the pulse time delay in picoseconds, and is a direct translation of twice the varying distance of the reference arm in the optical gating setup, Fig. 3. According to the diffusion model, the slope of the time-dependent transmission intensity is determined by the diffusion constant and the absorption length as given by Eq. (10). The decay times $\tau = 2.8$ ps for the 14-μm sample and $\tau = 1.0$ ps for the 7-μm sample, Fig. 10, are directly obtained from the slope of the fits.

The fits highlight the single exponential behavior of the data points with elapsed time. This implies an invariable diffusion constant, or constant diffusive transport of the 1500-nm light through the sample and is inconsistent with localization effects.

The thickness dependence of these decay times is plotted in Fig. 11. Two measurements on the same spatial spot on the sample were taken. Error bars in the graph is a result of the averaging of two measurements per thickness. Using the dynamic diffusive transport equation described in the decay time, Eq. (10), a fit was made through the data points. We use an inverse thickness factor, $[\pi/(L + 2z_e)]^2$, to plot the decay time progression with the inverse of the square of the effective thickness of the sample. In this way, the diffusion constant and the absorption length were directly obtained from the slope and the intercept. The diffusion constant and the absorption length were the free fitting parameters.

The red solid line through the data points shows the decay time equation fit. A diffusion constant of $D = 10 \pm 6$ m^2/s was obtained from the slope of the line, and the intercept gave the absorption length, $L_a = 6 \pm 2$ μm.

The results of the fit to Fig. 11 are reasonable with respect to both the absorption length and the energy velocity. The absorption length obtained here is consistent with the measurements of the total transmission and total reflection. The energy velocity v_e is related to the diffusion constant

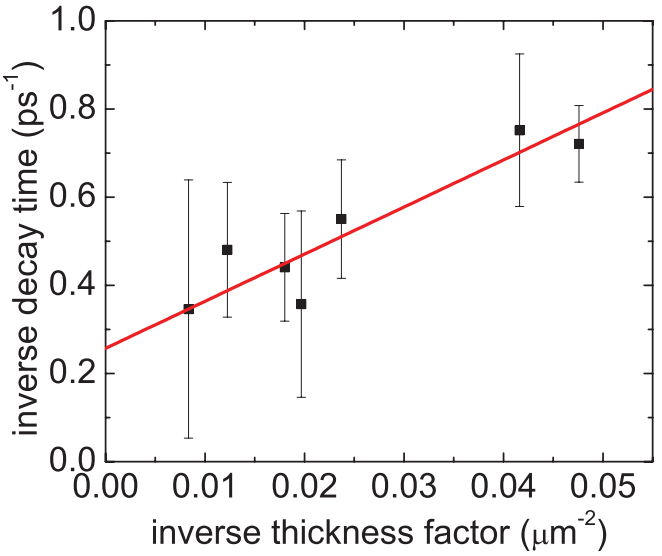

FIG. 11. (Color online) The inverse decay time obtained from the slopes of the exponential time resolved transmission measurements is plotted against the inverse thickness factor, $[\pi/(L+2z_e)]^2$. From Eq. (10), we then extract the diffusion constant from the slope, $D = 10 \pm 6$ m^2/s, and the absorption length from the intercept, $L_a = 6 \pm 2$ μm.

and the mean free path by $D = \frac{1}{3} v_e l$. Using this expression and the results obtained in our measurements gives an energy velocity of $1/6$ of the speed of light. The value of this reduced energy velocity is consistent with other work with powder samples.[33]

V. CONCLUSIONS AND DISCUSSION

Our results suggest that both the cw and time-resolved transport of light through ground GaAs powders can be fully described using the diffusion model. We observe an absorption length of 6.1 ± 1.9 μm and a transport mean free path of 0.6 ± 0.2 μm. Consistent values of the parameters were used for both cw and time-resolved measurements with the combination of measurements yielding a reasonable value for the energy velocity. These results shed new light on the absorption and localization debate of more than two decades ago.[11,12] The scattering strength, expressed by the product of wave vector and the transport mean free path, $kl = 5.5$ is according to the Ioffe-Regel rule[34,35] not in the regime where a transition into the Anderson localization is expected to take place. The mobility edge is however difficult to predict purely on the basis of basic experimental parameters. Two decades ago, e.g., Anderson localization results were invoked at a $kl \approx 40$.[36] Note that we have rightfully corrected the wave number by the effective refractive index. Our time-resolved transmission intensity exponential decay curves suggest the absence of Anderson localization in the GaAs ground samples investigated.

We have also presented a new way of depositing poly dispersed powders in a homogeneous fashion that may be useful for a range of powder characterization measurements that depend on homogenous thin layers of powders. We suspect that the cause of absorption is grinding-induced strain and/or defects in the sample as suggested by the x-ray scattering measurements. This grinding induced distortion of the crystal smears out the band-gap edge. The absorption was reduced somewhat by annealing the powder at a high temperature, but could not be eliminated entirely (see Appendix B).

We expect that this article will again spark the curiosity for the field of Anderson localization. New types of samples may open the door in the future for the experimental observation of 3D Anderson localization with electromagnetic waves.

ACKNOWLEDGMENTS

We thank the University of Amsterdam x-ray crystallography department for putting their facilities at our disposal, and University of Twente Mesa+ for measuring the x-ray SEM. We thank Nir Rotenberg and Jacopo Bertolotti for their contributions. This work is part of the research program of the "Stichting voor Fundamenteel Onderzoek der Materie" (FOM), which is financially supported by the Dutch organization for scientific research (NWO) and made possible by the Financial support by ENI-Donegani, Italy, and the European Network of Excellence on Nanophotonics for Energy Efficiency.

APPENDIX A: TIME-RESOLVED MEASUREMENTS OF INHOMOGENEOUS SAMPLES

The time-resolved transmission of samples with inhomogeneities was also measured. In the SEM images in Fig. 12, we show examples of two different samples with inhomogeneities. The image in Fig. 12(a) shows the interface between a region in the sample with pores in the order of 5 μm (left side) and a smoother part with virtually no pores (right side). Note that the pore size is orders of magnitude larger than the wavelength of the light used in the experiment. This sample was made using the drop drying deposition technique described in the methods section as opposed to the slow-drying technique that we ultimately used to make samples for the optical experiments. The SEM micrograph in Fig. 12(b) shows a part of a sample where we introduced a scratch with a blunt object to intentionally create an inhomogeneity. The scratch is approximately 40-μm wide in the center.

Both samples were used to compare time-resolved transmission measurements of the homogeneous and inhomogeneous regions in the optical gating setup.

Figure 13 shows the time-resolved transmission of light propagating through such an inhomogeneous region with a decreasing slope at longer times. The inset of the graph is the measurement on the unscratched part of the sample in Fig. 12(b), on the top right side of the scratch. From the curves, we estimated the diffusion constant and the transport mean free path (see Table I). When the laser beam is partly on the scratched part of the sample, the diffusivity expressed by a changing diffusion "constant" varies between 64 ($t = 1.4$ ps) and 37 m^2/s ($t = 12.4$ ps). The latter is also the diffusion constant of the single exponential curve obtained in the

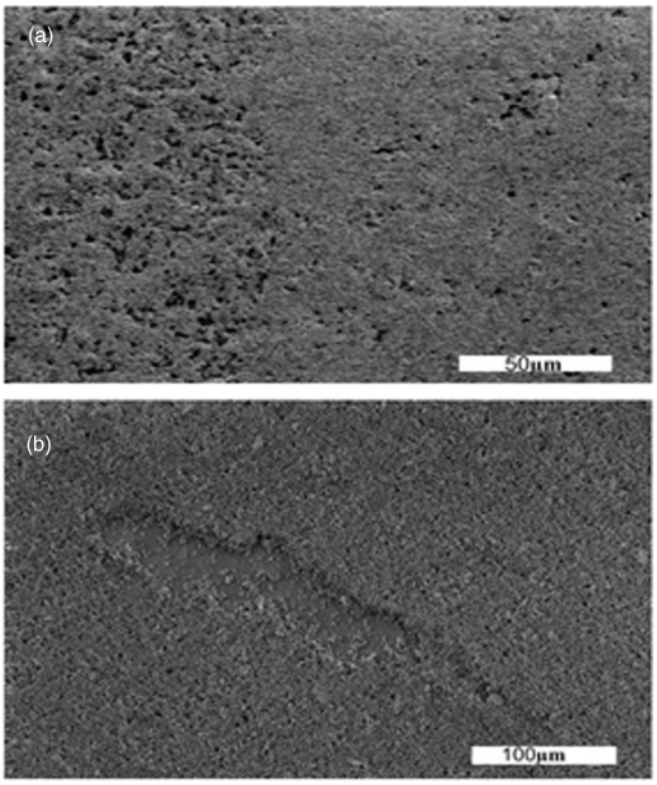

FIG. 12. SEM images of an inhomogeneous GaAs powder sample (a) and a sample where we introduced a scratch with a blunt object, uncovering the glass substrate surface (b). Note that the top SEM image (a) contains two regions, created when the sample was sedimented. The left region has more and larger pores than the right region.

homogeneous region of the same sample (see inset of Fig. 13). We attribute the changes in the curve to internal reflections

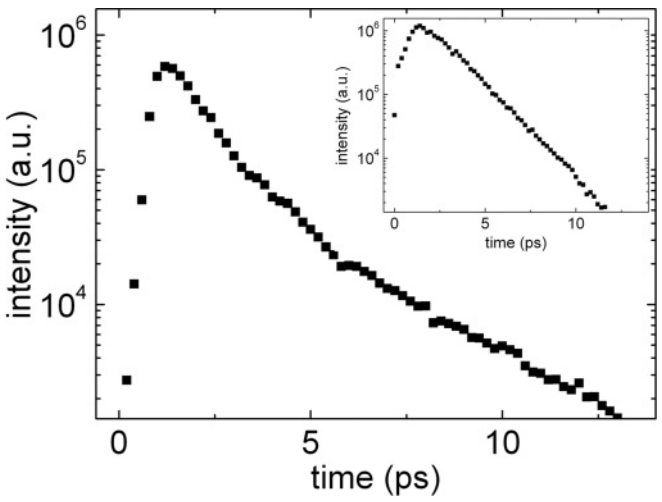

FIG. 13. Logarithmic plots of time-resolved transmission measurements of a 34-μm-thick sample fabricated by drop-drying deposition. The inhomogeneous surface, thickness differences, and large voids cause nonexponential behavior, as shown in the large graph. The inset shows the measurement on a different location of the same sample where the surface is smooth and particles well distributed in the order of the particle size average.

TABLE I. Physical properties of a homogeneous and an inhomogeneous sample with comparable thicknesses. The values were obtained from the time-resolved decay curves. The sample with a homogeneous thickness distribution and a sample with inhomogeneous thickness distribution. L is the thickness of the sample, l the measured mean free path extracted from total transmission data, D the diffusion constant from the time-resolved transmission measurements, and T the combination of the diffusive total transmission and the ballistic transmission at $\lambda = 1.5$ μm.

Sample	Decay	L	l (μm)	D (m^2/s)	T
inhomog.	nonexp.	34	2.0 ± 0.4	64–37	0.15
homog.	exp.	34	0.5 ± 0.1	37	0.05

in the sample because of the large pores and voids in the sample. The diffusion constant changes as it travels different path lengths. Table I shows that if scratches or holes in powder samples are overlooked, the diffusion constant and the mean free path can be overestimated, giving rise to errors in the interpretation. We emphasize the importance of thorough sample characterization.

When the region of the same sample is completely smooth and compact, as shown in the inset of Fig. 13 with a constant thickness in the measured area, the decay curve typically showed an exponential dependence with time.

APPENDIX B: POWDER POST-TREATMENT

Two batches of powders here heated to high temperature in an attempt to anneal the grinding induced defects from the GaAs powder and thus reduce absorption. As shown in the table below (see Table II), annealing did reduce the absorption length from 7 to 11 μm. L_a was obtained by filling in the equations for the total transmission, the total reflection, and the ballistic transmission (explained in the theory section of the article) with the experimental values in the table below (see Table II). Note that the value for the ballistic transmission is included in the T measurements in Table II. The powder annealed at 900 °C is not further analyzed after the measurement of a lower reflectivity.

TABLE II. Comparison between a non-annealed and annealed sample of nearly same thickness. R is the total reflection and T the combination of the diffusive total transmission and the ballistic transmission at $\lambda = 1.5$ μm. The absorption lengths were determined through the total transmission and reflection data. The annealing of the powder at 700 °C decreased the absorption in the sample notably. For reasons not investigated, the total reflection of the 900 °C annealed GaAs powder is lower than the other samples.

Sample	L (μm)	R	T	L_a (μm)
not annealed	48	0.50	0.06	7 ± 2
700 °C annealed	53	0.67	0.10	11 ± 4
900 °C annealed	35	0.52	0.09	9 ± 3

*tvanderbeek@amolf.nl

[1] L. E. McNeil and R. H. French, Acta Mater. **48**, 4571 (2000).
[2] M. Law, L. E. Greene, J. C. Johnson, R. Saykally, and P. Yang, Nat. Mater. **4**, 455 (2005).
[3] R. R. Anderson and J. A. Parrish, J. Invest. Dermatol. **77**, 13 (1981).
[4] P. W. Anderson, Phys. Rev. Lett. **109**, 1492 (1958).
[5] D. J. Thouless, Phys. Rep. **13**, 93 (1974).
[6] M. P. van Albada and A. Lagendijk, Phys. Rev. Lett. **55**, 2692 (1985).
[7] P. E. Wolf, G. Maret, E. Akkermans, and R. Maynard, J. Phys. **49**, 63 (1988).
[8] B. Shapiro, Phys. Rev. Lett. **57**, 2168 (1986).
[9] C. M. Aegerter, M. Störzer, W. Bührer, S. Fiebig, and G. Maret, J. Mod. Opt. **54**, 2667 (2007).
[10] D. S. Wiersma, P. Bartolini, A. Lagendijk, and R. Righini, Nature (London) **390**, 671 (1997).
[11] F. Scheffold, R. Lenke, R. Tweer, and G. Maret, Nature (London) **398**, 206 (1999).
[12] D. S. Wiersma, J. Gómez Rivas, P. Bartolini, A. Lagendijk, and R. Righini, Nature (London) **398**, 207 (1999).
[13] J. Gómez Rivas, R. Sprik, A. Lagendijk, L. D. Noordam, and C. W. Rella, Phys. Rev. E **63**, 046613 (2001).
[14] M. Störzer, P. Gross, C. M. Aegerter, and G. Maret, Phys. Rev. Lett. **96**, 063904 (2006).
[15] C. M. Aegerter, M. Störzer, and G. Maret, Europhys. Lett. **75**, 562 (2006).
[16] M. P. van Albada, M. B. van der Mark, and A. Lagendijk, Phys. Rev. Lett. **58**, 361 (1987).
[17] P. E. Wolf and G. Maret, Phys. Rev. Lett. **55**, 2696 (1985).
[18] M. P. van Albada, J. F. de Boer, and A. Lagendijk, Phys. Rev. Lett. **64**, 2787 (1990).
[19] F. Scheffold and G. Maret, Phys. Rev. Lett. **81**, 5800 (1998).
[20] W. Bührer, T. Sperling, S. Gentilini, C. M. Aegerter, and G. Maret, Poster at conference *"Mesoscopic Physics in Complex Media,"* Cargèse, France, 2010.
[21] J. Gómez Rivas, R. Sprik, C. M. Soukoulis, K. Bush, and A. Lagendijk, Europhys. Lett. **48**, 22 (1999).
[22] S. E. Skipetrov and B. A. van Tiggelen, Phys. Rev. Lett. **96**, 043902 (2006).
[23] H. Hu, A. Strybulevych, and J. H. Page, Nat. Phys. **4**, 945 (2008).
[24] A. Ishimaru, *Wave Propagation and Scattering in Random Media* (Academic, New York, 1978).
[25] A. Lagendijk, R. Vreeker, and P. de Vries, Phys. Lett. A **136**, 81 (1989).
[26] J. X. Zhu, D. J. Pine, and D. A. Weitz, Phys. Rev. A **44**, 3948 (1991).
[27] J. Gómez Rivas, Ph.D. thesis, University of Amsterdam, the Netherlands, 2001.
[28] G. A. Niklasson, C. G. Granqvist, and O. Hunderi, Appl. Opt. **20**, 26 (1981).
[29] P. Sheng, *Introduction to Wave Scattering, Localization, and Mesoscopic Phenomena* (Academic, New York, 1995).
[30] A. L. Patterson, Phys. Rev. **56**, 978 (1939).
[31] R. H. J. Kop, P. de Vries, R. Sprik, and A. Lagendijk, Phys. Rev. Lett. **79**, 4369 (1997).
[32] M. Bellingeri, S. Longhi, and F. Scotognella, J. Eur. Opt. Soc. **5**, 10041 (2010).
[33] M. P. van Albada, B. A. van Tiggelen, A. Lagendijk, and A. Tip, Phys. Rev. Lett. **66**, 3132 (1991).
[34] A. F. Ioffe and A. R. Regel, Prog. Semicond. **4**, 237 (1960).
[35] E. Abrahams, P. W. Anderson, D. C. Licciardello, and T. V. Ramakrishnan, Phys. Rev. Lett. **42**, 673 (1979).
[36] P. M. Platzman and M. Y. Azbel, Phys. Rev. B **36**, 2350 (1987).